

Solving the Bethe-Salpeter equation on massively parallel architectures

Xiao Zhang^{a,**}, Sebastian Achilles^{b,c}, Jan Winkelmann^c, Roland Haas^d, André Schleife^{d,e,f,**}, Edoardo Di Napoli^{b,*}

^aDepartment of Mechanical Science and Engineering, University of Illinois at Urbana-Champaign, Urbana, IL 61801, USA.

^bJülich Supercomputing Centre, Forschungszentrum Jülich, Wilhelm-Johnen-Straße, 52425 Jülich, Germany.

^cRWTH Aachen University, Aachen Institute for Advanced Study in Computational Engineering Science, Schinkelstr. 2, 52062 Aachen, Germany.

^dNational Center for Supercomputing Applications, University of Illinois at Urbana-Champaign, Urbana, IL 61801, USA.

^eDepartment of Materials Science and Engineering, University of Illinois at Urbana-Champaign, Urbana, IL 61801, USA.

^fMaterials Research Laboratory, University of Illinois at Urbana-Champaign, Urbana, IL 61801, USA.

Abstract

The last ten years have witnessed fast spreading of massively parallel computing clusters, from leading supercomputing facilities down to the average university computing center. Many companies in the private sector have undergone a similar evolution. In this scenario, the seamless integration of software and middleware libraries is a key ingredient to ensure portability of scientific codes and guarantees them an extended lifetime. In this work, we describe the integration of the ChASE library, a modern parallel eigensolver, into an existing legacy code for the first-principles computation of optical properties of materials via solution of the Bethe-Salpeter equation for the optical polarization function. Our numerical tests show that, as a result of integrating ChASE and parallelizing the reading routine, the code experiences a remarkable speedup and greatly improved scaling behavior on both multi- and many-core architectures. We demonstrate that such a modernized BSE code will, by fully exploiting parallel computing architectures and file systems, enable domain scientists to accurately study complex material systems that were not accessible before.

Keywords: Eigensolver, exciton Hamiltonian, parallel computing, high-performance computing, code modernization

1. Introduction

As the size of massively parallel computing clusters is advancing towards the exascale regime, utilizing the great power of such clusters for scientific applications is a very important task. In the last decade, modernizing domain-specific software by improving its parallelism and efficiency has grown into a mainstream activity in many fields of computational scientific research. Co-design and portability is playing an ever increasing role in coordinating the effort

in pushing the development of new hardware, efficient middleware, such as numerical libraries, and their use to run massively parallelized simulations [1, 2, 3, 4]. In this paper, we present a notable example of such an effort. We describe how the initialization of a large and dense Hermitian eigenproblem and the solution for a small portion of its spectrum are the two major bottlenecks in the parallel execution of an existing code [5, 6] for solving the Bethe-Salpeter equation (BSE) [7, 8]. We illustrate how we improve the parallel I/O and integrate a modern highly parallelized solver—the Chebyshev Accelerated Subspace Iteration Eigensolver (ChASE) [9]—into the solution of the BSE. Besides increased performance and parallelism, we demonstrate that our implementation allows the code to tackle physical problems that could not be addressed before.

In the context of this work, the solution of the BSE equation is used to study the response of a ma-

*Principal corresponding author

**Corresponding author

Email addresses: xzhng125@illinois.edu (Xiao Zhang), s.achilles@fz-juelich.de (Sebastian Achilles), winkelmann@ices.rwth-aachen.de (Jan Winkelmann), rhaas@ncsa.illinois.edu (Roland Haas), schleife@illinois.edu (André Schleife), e.di.napoli@fz-juelich.de (Edoardo Di Napoli)

material to an external electromagnetic field—including visible light—and in so doing derive the material optical properties. Accurate and predictive modeling of optical response is important, for instance, to understand the functionality of optoelectronic devices, whose applications are directly related to light absorption, reflection, and transmission. For instance, creation or separation of excitons is an important process in photovoltaic cells and light-emitting diodes [10, 11]. Upon optical excitation via an electromagnetic field, electrons in a material leave their original electronic ground state, gain energy, and reach an excited state. This process leaves a positively charged hole in the initially occupied valence state. The electrons and holes couple via the Coulomb interaction as they propagate, rendering this situation an intricate electron-hole quantum mechanical problem that is much more complicated than the ground state.

While these optical properties can be measured experimentally by approaches including ellipsometry [12], photoluminescence [13], and photoemission [14], accurate predictive studies are crucial in interpreting experiments and guiding research towards successful discovery of materials for different applications. Such predictive *in silico* studies of optical properties require a description of excited electronic states and are carried out using first-principles approaches that solve approximations to the fundamental Schrödinger equation in a non-parametric fashion. This would then allow one to carry out quantitative simulations to compute material properties. The BSE approach is based on many-body perturbation theory (MBPT) and is a common first-principles method to simulate the underlying optical absorption strength and its energy dependence accurately.

This Green’s function based approach considers the external electric field as a perturbation to the electronic ground state and describes the response of the electronic system to such a perturbation. Key to the effectiveness of the approach is that it accounts for the *screened* Coulomb interaction between the electron and the hole, and thus gives an accurate account of the optical excitation process. However, one of the main challenges of this approach lies in its extremely large computational cost which scales as $\mathcal{O}(n_e^6)$ [15], where n_e is the number of electrons in the material. Although this can be reduced to $\mathcal{O}(n_e^3)$ or even $\mathcal{O}(n_e^2)$ with advanced solvers [15, 5], studying large or complicated material systems using the BSE approach is still limited by the large size of the corresponding

eigenproblem, which can go up to $\mathcal{O}(10^6)$.

In the last decade, tier-0 computing clusters have grown to the point of having hundreds of thousands of computing cores with peak performances up to hundreds of Peta-FLOPS (Floating Point Operations per Second). Such massively parallel architectures have the potential to tackle and solve eigenproblems significantly larger than $\mathcal{O}(10^6)$. Therefore, solving for the largest BSE is quite within the capability of the available hardware. The real challenge is the ability of numerical libraries to take advantage of such computing resources and parallelize efficiently over many thousands of cores for a given eigenproblem.

One of the disadvantages of dense eigenvalue solvers is that their complexity usually scales as the cubic power of the matrix size N , while their memory footprint grows as N^2 . This limits the rapid scaling of the problem size to a large number of computing cores. On the other hand, in many important cases the BSE eigenproblem has to be solved for a very small fraction of its spectrum, usually comparable to or less than 1 % of its total size.

Numerical libraries such as ScaLAPACK [16] or the more modern SLATE [17] maintain a very high complexity even in those cases where the used algorithm can compute a portion of the spectrum—e.g. the MRRR eigensolver. Conversely, iterative eigensolvers, such as Conjugate Gradient (CG) [18, 19] or Lanczos [20], could in principle have a lower complexity closer to N^2 . When implemented in iterative libraries such as SLEPc [21] or Trillinos [22], these iterative algorithms pay the price of a smaller arithmetic intensity. Few operation per byte are executed with the result that the processor remains idle waiting for the necessary data to be moved through the memory hierarchy. The resulting number of operations per second is rather low with respect to the peak performance of the CPU. It is customary to refer to the executed operations as “slow” FLOPs¹.

In this paper we argue that there are alternatives to both high complexity and “slow” FLOPs. We show how a modern library based on subspace iteration and augmented with Chebyshev filter can be a winning alternative in cases where a limited portion of the spectrum of a large dense eigenvalue problem is desired. The ChASE library has a complexity of $\mathcal{O}(mN^2)$, with m proportional to the number of eigen-

¹To be distinguished from FLOPS which is a rate of operations per second

pairs sought after. When $m \ll N$, ChASE executes a number of operations to compute the solution that is substantially smaller than $\mathcal{O}(N^3)$. At the same time, most of the ChASE floating point operations ($\sim 90\%$) are executed using BLAS level 3 subroutines that are known to extract most of the peak performance out of any existing parallel computing architecture.

We integrated the highly parallelized ChASE library with an existing BSE code that has its origin in the group of Friedhelm Bechstedt at the Friedrich-Schiller University Jena, where it was developed over many years [23, 24]. It is closely developed around the Vienna Ab-Initio Simulation Package (VASP) and its implementation is described in Refs. [5, 6]. The integration of ChASE leads to significant improvement when the BSE code is executed on massively parallel clusters. On a given set of computing resources, the gain in adopting ChASE can exceed a factor of 4–5 in runtime compared to the previously used CG solver. Comparing the parallel efficiency of both solvers supports such result: ChASE’s efficiency curve maintains much higher values than CG as the number of computing nodes increases. In addition, the higher performance outcome of ChASE allows us to explore material systems where the previous implementation could not fully unravel the sought after physics. We illustrate this feature by looking into the extraction of accurate optical properties of the organic crystal naphthalene.

The paper is organized as follows. In Sec. 2, we explain the details of the BSE approach and describe the challenges of dealing with the BSE problem due to the necessity of solving large size matrices. In Sec. 3, we illustrate how such challenges appear in our existing BSE code, both in the I/O procedure and the eigensolver and explain the many benefits of the new I/O routine and the ChASE solver. In Sec. 4, we describe numerical experiments to measure the strong and weak scaling and illustrate the power of ChASE in addressing optoelectronic properties of complex materials. Section 5 summarizes and concludes the paper.

2. Modeling the Optical Properties of Materials

Solving the Bethe-Salpeter equation (BSE) [7] for the optical polarization function defines a theoretical spectroscopy approach that accounts for two-particle, electron-hole excitations, by including the interaction between excited electrons and holes using many-body

perturbation theory [8]. It is a first-principles framework used to accurately predict fundamental optical properties, such as optical absorption spectra including excitonic effects and exciton binding energies for molecules, semiconductors, and insulators. The exciton binding energy is defined as the difference between interacting and non-interacting electron-hole pair energies and corresponds to the energy required to separate a bound electron-hole pair.

The BSE is based on a Green’s function technique to describe the electron-electron interaction and can be derived from Hedin’s system of equations [25] via an expansion of the electronic self energy Σ into increasing orders of the screened electron-electron interaction W [26, 27]. For numerical implementations the solution of the BSE is transformed into an eigenvalue problem $\hat{H}^{\text{BSE}}|\Lambda\rangle = E_\Lambda|\Lambda\rangle$, with the exciton Hamiltonian [8, 27, 5]

$$\hat{H}_{v\mathbf{c}\mathbf{k},v'\mathbf{c}'\mathbf{k}'}^{\text{BSE}} = (E_{\mathbf{c}\mathbf{k}} - E_{v\mathbf{k}})\delta_{vv'}\delta_{cc'}\delta_{\mathbf{k}\mathbf{k}'} + 2\bar{v}_{v\mathbf{c}\mathbf{k}}^{v'\mathbf{c}'\mathbf{k}'} - W_{v\mathbf{c}\mathbf{k}}^{v'\mathbf{c}'\mathbf{k}'}.$$
(1)

Here, the c , v , and \mathbf{k} indices label conduction bands, valence bands, and points in reciprocal space, respectively. $E_{\mathbf{c}\mathbf{k}}$ and $E_{v\mathbf{k}}$ are energies of single-(quasi)particle electron and hole states and are computed by applying quasiparticle corrections to Kohn-Sham eigenvalues from ground-state density-functional theory [28, 29]. It is common practice to compute these using one of two approaches: (i) The single-quasiparticle Green’s function scheme within many-body perturbation theory, known as the *GW* approximation of the electronic self energy [25, 8], or (ii) hybrid exchange-correlation functionals in a generalized Kohn-Sham scheme [30]. Finally, the unscreened Coulomb interaction, denoted by \bar{v} in Eq. (1), represents short-range electron-hole exchange to account for local-field effects. W denotes the screened Coulomb interaction and requires an approximation and numerical description of dielectric screening.

Solving the BSE numerically is computationally intensive: The \bar{v} and W terms involve coupling between all electron-hole pairs and, as can be seen from Eq. (1), the rank of the BSE Hamiltonian depends on the number of (occupied) valence bands, (unoccupied) conduction bands, and the \mathbf{k} -point sampling of reciprocal space. Of these, the number of occupied bands is determined by the number of electrons in the simulation cell for a given material. However, the number of conduction bands and sampling of reciprocal space are convergence parameters. While finer reciprocal-space

sampling and more conduction bands lead to better converged solutions of the BSE, this increases the size of the BSE Hamiltonian. In practice, one examines the convergence of physical quantities, such as the exciton-binding energy, with respect to a finite-sized sampling of reciprocal space. To limit the number of empty states taken into account for the Hamiltonian, a BSE energy cutoff E_{cut} is introduced such that only electron-hole pairs with $E_{c\mathbf{k}} - E_{v\mathbf{k}} < E_{\text{cut}}$ contribute. Effects from electron-hole pairs with higher energies are typically small due to decreasing coupling \bar{v} and W and, therefore, can be neglected. However, it needs to be tested what value for E_{cut} achieves a certain convergence level, e.g. for the exciton-binding energy.

Even when \mathbf{k} -point sampling and BSE energy cutoff are carefully converged, the resulting eigenproblem can become very large. Its size increases linearly with the number of conduction bands, valence bands, and \mathbf{k} -points, as more non-interacting conduction-valence band pairs are included. Depending on the exact goals of a simulation, e.g. whether just exciton binding energies or an entire spectrum are of interest, the typical test range for the BSE cutoff is on the order of 5–20 eV. The precise increase of the rank of the BSE matrix depends on details of the electronic band structure of a material, and it typically increases a few orders of magnitude across this energy range, from several thousands to close to half a million. For instance, in previous work we demonstrated that solving for eigenproblems with size as large as 360,000 is necessary to obtain reasonable results for the convergence with respect to \mathbf{k} -point sampling [5, 31, 32, 33].

As an illustration, we describe below our previous work on optical properties of a meta-stable ZnO polymorph [33]. To converge exciton binding energies with respect to \mathbf{k} -point sampling, we follow the procedure of Ref. [5]: For a number of samplings, the calculated binding energy is plotted as a function of the inverse number of \mathbf{k} -points. The convergence in such a plot shows linear behavior for very dense \mathbf{k} -point samplings, which allows an extrapolation to estimate the exciton-binding energy at infinitely dense sampling. For ZnO, this linear regime is not observed until the inverse number of \mathbf{k} -points is smaller than 0.015, corresponding to 66.7 \mathbf{k} -points in one specific reciprocal-space direction (see details in Ref. [33]). The smallest inverse number of \mathbf{k} -points that we studied for this material in Ref. [33], i.e., the densest \mathbf{k} -point sampling, is 0.012, corresponding to 83.3 \mathbf{k} -points in that

direction. This leads to an eigenvalue problem with a size of $\sim 200,000$ and reading such a matrix and solving for 100 eigenvalues using the KSCG solver required 5–6 hours using 32 nodes of the BlueWaters supercomputer. Pushing towards better convergence with respect to \mathbf{k} -point sampling becomes expensive quickly: Reducing the inverse number of \mathbf{k} -points to 0.010 increases the matrix size to $\sim 300,000$ and requires more than twice the memory.

The increase in matrix size is even more dramatic for more complex materials. While the primitive unit cell of ZnO contains only four atoms and 36 valence electrons, these numbers can easily be one order of magnitude larger. For instance, the unit cell of In_2O_3 [32] contains 16 In and 24 O atoms, leading to 352 valence electrons. In this case the matrix rank already amounts to $\sim 360,000$ using a $5 \times 5 \times 5$ \mathbf{k} -point grid and $E_{\text{cut}} = 12.5$ eV. Hence, computing converged optical spectra constitutes a serious computational problem, since it requires a converged \mathbf{k} -point grid *and* a large BSE energy cutoff. In this case, the BSE cutoff is determined by the maximum energy in the spectrum, which is typically much larger than what is needed to merely converge excitonic effects. We mitigate this issue by using dense \mathbf{k} -point grids for the low energy range where a smaller BSE cutoff is sufficient, and more coarse \mathbf{k} -point grids for large photon energies, which requires large BSE cutoffs (see e.g. Ref. [32] for optical spectra of In_2O_3). However, for materials with large unit cells, such as the organic crystal naphthalene $\text{C}_{20}\text{H}_{16}$ (see Sec. 4.4), computing exciton binding energies leads to large matrices on the order of 5×10^5 when converging E_{cut} and \mathbf{k} -point sampling.

When computing exciton binding energies of a material, only a very small portion of the lower eigenspectrum is needed. This is because studies of excitonic properties typically focus on states at or near the absorption edge, corresponding to the lowest eigenvalues of the BSE matrix. When only few extremal eigenpairs are computed, it is customary to use iterative solvers even when the matrix defining the eigenproblem is dense. Such a choice is in part influenced by the overall complexity of the iterative algorithm compared with a so-called direct one (e.g. Multiple Relatively Robust Representations [34, 35]). In an iterative solver the total number of floating point operations to reach the solution, is determined by the complexity of the algorithm per iteration multiplied by the number of iterations needed to converge. Since the overall number of iterations is unknown a priori,

the choice of iterative vs. direct solver depends on the properties of the eigenproblem, the parameters of the solver and its parallel efficiency, and is often a question of practice and experience.

In our BSE code we relied on an iterative solver based on the Kalkreuther-Simma Conjugate-Gradient (KSCG) algorithm[5, 36] to solve increasingly larger BSE eigenproblems. While this algorithm presents clear advantages with respect to any direct solver, it lags behind when it is employed over increasingly larger parallel platforms. In the next section, we dig into the reasons for such lack of parallel performance and propose a modern alternative which is more efficient, scales over massively parallel architectures, and enables us to tackle eigenproblems of unprecedented size.

3. The Computational Challenges

The overall workflow towards the solution of a single BSE starts with a density functional theory calculation to obtain single-particle Kohn-Sham states and dipole matrix elements. We perform these steps using the Vienna Ab initio Simulation Package (VASP) [37, 38, 39]. The VASP code is a commercial open-source code commonly used for first-principles calculations, and provides reliable results to compute the electronic structures of materials. The Kohn-Sham electronic structure and quasiparticle corrections are then used to compute the BSE Hamiltonian, Eq. (1). Subsequently, either the lowest eigenvalues of the BSE matrix are extracted by using an eigensolver based on the Conjugate Gradient algorithm [36] or optical spectra are computed using the time-propagation technique described in Refs. [23, 24].

3.1. A brief introduction to the BSE code

To obtain the solution to the BSE eigenvalue problem, there are two main stages that necessitate a large amount of computational resources: the initialization of the BSE Hamiltonian and the computation of the lowest portion of its spectrum. In our BSE implementation, described in detail in Refs. [6, 5], the initialization is split into two steps: 1) the generation of the matrix elements as they are represented in Eq. (1) and the assembly of the matrix in main memory as input for the solver. The workflow for the first step of the initialization is embarrassingly parallel since there is no communication between different threads. Thanks

to the fact that the matrix elements in the BSE eigenvalue problem are independent of each other, the matrix elements are evaluated in chunks, where every subset of the matrix is computed independently from the others. The user specifies the total number of jobs used to write the full matrix. The calculation of the matrix elements is split between these multiple independent jobs, each parallelized over one entire node using OpenMP and writing a portion of the matrix on individual binary files. In the second step, after all matrix elements are calculated and stored, a separate procedure reads in the matrix elements and performs the diagonalization (to compute eigenvalues) or a time-propagation scheme (to compute the dielectric function). This scheme is beneficial if multiple different diagonalizations are to be performed on the same matrix, e.g. for convergence tests as described in Ref. [5]. Furthermore, as long as the time spent writing and reading the matrix is small compared to initialization and diagonalization steps, this scheme also allows efficient writing of large matrices using many single-node jobs and benefiting from backfill algorithms of modern queuing systems. The workflow above is implemented in our BSE code [5, 6] discussed here.

As an illustration, calculating the matrix elements for the ZnO system [33] for a matrix of size 199,433 requires about 600 node hours on Blue Waters, while reading the matrix and computing the lowest 100 eigenvalues requires 39 node hours, and 48 node hours (i.e., 87.3%, 5.7%, and 7.0%), respectively. The step of computing the matrix elements can be trivially parallelized on as many nodes as necessary. However, the rest of the computational time is roughly split in half between I/O and solution of the eigenproblem. Furthermore, in some of our tests the I/O alone required close to the maximum walltime on BlueWaters, making it challenging to complete these runs. Consequently, the main challenges in improving the code lays in increasing the performance and parallelism of these two tasks. In the following part of this section, we introduce the new parallel reading process of the matrix elements to replace the old sequential reading process, and a new sub-space iterative solver to improve the parallel efficiency in computing the solution with respect to the conjugate gradient solver.

3.2. Matrix generation and the I/O challenge

As discussed above, in step one each independent thread computes a number of rows of the exciton

Hamiltonian matrix, Eq. (1), and writes these to a single file. Next, these individual files are read and the data is distributed amongst several MPI ranks for the subsequent solver step. The existing implementation serialized reading data from files by assigning a “reader” rank to each file and allowing only one reader to read at any given time. After completing reading its assigned file, the reader would broadcast the read data to all ranks, which would use the received data to fill in their local part of the full matrix. Once the broadcast is completed, the next reader would read its assigned file until all files were read and broadcast. This algorithm proved to be a bottleneck when assembling large matrices on massively parallel clusters like Blue Waters.

Hence, for this work we extended the reader code to be split in two phases “reading from disk” (I/O) and “completing the matrix” (communication). Doing so avoids the need to serialize during the I/O phase. We designed the algorithm to support any desired number of MPI ranks reading concurrently, as long as the file system can sustain the concurrent reads. Once the Hermitian matrix is read, the upper half is filled by sending data from those ranks that read the corresponding transposed part. This completely avoids serialization while reading and introduces only a small amount of serialization while sending data between ranks due to our use of blocking MPI calls. With this new approach the total time spent to read and complete the matrix is almost identical to the raw I/O time on the “reader” rank reading the largest file, indicating that MPI communication is not a significant part of the time budget. Finally, when using ChASE to diagonalize the parallel matrix, the matrix needs to be converted from being distributed purely along rows (“stripped”) to being distributed in blocks (“blocked”). For the current usage scenario there is sufficient memory available to store both the striped and the blocked copy of the matrix, permitting the use of a simple out-of-place algorithm using blocking MPI one-to-one communication calls to redistribute the matrix data among the MPI ranks. Overall, these changes resulted in a significant speedup by reducing time spent to read and build the matrix (see Table 1 for detailed results).

3.3. Solving the BSE eigenvalue problem on massively parallel architectures

The BSE Hamiltonian matrix is both dense (most of its entry are non-zero) and large with a size N up

to 10^6 . When dealing with dense Hermitian matrices, it is customary to use a so-called “direct” eigensolver, which computes solutions by directly reducing the form of the matrix to tri-diagonal form. Afterwards an iterative solver is used to further transform the matrix to diagonal, to recover its real eigenvalues.

When only a small number $m \ll N$ of low-lying eigenvalues is sought, it is customary to resort to iterative eigensolvers, which are typically used in the case of sparse matrices. The main reason for this choice resides in the fact that the number of floating point operations needed to compute the solution is $\mathcal{O}(N^2m)$, which can be much smaller than the $\mathcal{O}(N^3)$ operations required by a direct eigensolver. The break-even point between these two classes of algorithms depends on the number of iterations needed by the iterative algorithm to declare all desired eigenpairs converged.

The eigenvectors of the BSE Hamiltonian represent physical low-lying eigenmodes and provide information on the single-particle excitations that contribute to a given excitonic state. Hence, we are interested in the full eigenpairs not just the low-lying eigenvalues. In this case, it is advisable to use an iterative eigensolver based on a subspace projection. The main rationale is that such an algorithm deals with the entire set of desired eigenvectors instead of converging each one in a sequential fashion, as it is typical for Krylov space methods [40, Ch. 9]. The advantage of subspace methods is that the search space for the eigenvectors can be treated as one contiguous block and further refined at each iteration of the eigensolver. This is the main philosophy behind the version of the Conjugate Gradient (CG) method [18, 19] modified by Kalkreuter and Simma (KSCG) in their work [36].

The advantage of CG with respect to the classic Lanczos algorithm is in its ability to return eigenvalues with controlled numerical errors and correct multiplicities. Kalkreuter and Simma improved the CG algorithm by alternating CG minimization with direct minimization of the subspace spanned by the approximate eigenvectors. The KSCG solver yields a computational cost in terms of FLOP count that scales as $\mathcal{O}(N^2mC_0)$, where C_0 is the total number of CG cycles to converge all desired m eigenpairs. In KSCG the number of needed CG cycles grows with larger eigenvalues and is determined dynamically at runtime. Therefore it is not possible to have an *a priori* estimate of it. Nonetheless the total FLOP count is greatly reduced from the $\mathcal{O}(N^3)$ needed for the exact diagonalization of the matrix.

Originally conceived for applications in Quantum Chromodynamics, the KSCG eigensolver parallel implementation is based on geometrical data decomposition where vectors are equally partitioned and stored on distinct processing nodes. This choice was based on the assumption that the matrix of the eigenproblem is sparse and local, implying communication only between nearest-neighbor nodes for matrix-vector multiplications.

With the adoption of the KSCG algorithm, our BSE code had been applied to successfully study excitonic properties for many material systems, see e.g. Refs. [41, 42] and references therein. Unfortunately, because the BSE Hamiltonian is dense and lacks a local structure, the KSCG eigensolver ends up having a much larger inter-node communication load both in terms of message size and number of MPI collectives calls. We also note that each CG cycle deals with a vector at a time which implies that the arithmetic intensity (the number of operations per byte) of the algorithm is relatively low. Typically such an algorithm is bound by memory bandwidth and has a performance far from the theoretical peak of the processor. For these reasons KSCG suffers from limited parallel scalability. In turn, such a limitation curbs the amount of parallel resources that can be used effectively, and restricts the usage of our BSE code to investigate large physical systems which could be simulated on modern massively parallel architectures with thousands of compute cores.

The challenge of efficient use of parallel computing resources when solving large dense eigenvalue problems is not new. Several attempts have focused on improving direct methods [43, 44, 45] that are, in part, based on kernels with a high arithmetic intensity which exploit the multi-core processor performance. A typical example is the operation of reduction of a dense matrix to banded form which is based on the *fast FLOPs*² of Basic Linear Algebra Subroutines level 3 (BLAS-3) kernels [44]. These kernels are the most optimized in numerical linear algebra libraries [46, 47, 48] and can achieve up to 95% of the theoretical peak performance of the processor. Despite their recent advances all direct solvers are limited by the intrinsic computational complexity of their approach which scales as $\mathcal{O}(N^3)$ and limits their effective parallelization.

²The term “fast FLOPs” here is the opposite as the term “slow FLOPs” already defined in the introduction.

Our aim is to keep the advantage of fast FLOPs and to reduce the complexity of the eigensolver. To our knowledge, the only recent development in the field of numerical linear algebra that can achieve both goals is the Chebyshev Accelerated Subspace iteration Eigensolver (ChASE) [9]. This eigensolver has been initially developed to solve sequences of dense eigenproblems as they arise in Density Functional Theory (DFT) based on plane waves. The effectiveness of ChASE stems from a spectral filter based on Chebyshev polynomials. These polynomials can be computed through a 3-term recurrence relation, which enables the filter to be expressed in terms of BLAS-3 kernels. In addition, the fraction of computational time spent in the filter is by far larger than any other task within ChASE. This makes ChASE an extremely efficient solver in terms of node-level performance.

When parallelized over multiple nodes, ChASE takes advantage of its simple algorithmic structure based on subspace iteration and matrix-matrix multiplication to keep the amount of communication to an acceptable level. In practice, the BSE matrix is distributed only once across all MPI ranks in equal blocks of data and never re-distributed. Communication through MPI collective calls involves only the matrix of filtered vectors spanning the subspace. It has been shown [9] that communication overhead is minimized whenever the number of MPI ranks can be arranged in a square Cartesian grid. Performance is achieved, at the node-level, by using specialized multi-threaded libraries such as MKL or cuBLAS (for computation on GPU cards). Finally, ChASE allows pre-computing and minimizing the total FLOP count necessary to reach convergence.

Because the ChASE library and the BSE code are written in C++ and Fortran, respectively, the integration and usage of ChASE as the eigensolver necessitated the implementation of a glue code and, as described in Sec. 3.2, the initialization and distribution of the BSE Hamiltonian had to be reworked to be compatible with the data layout of ChASE. This also reduced the time spent in I/O and redistribution of data. ChASE requires the choice of a variable which sets the size of the search subspace which is a superset of the subspace spanned by the desired eigenvectors of the BSE matrix. As we will see in the next section (and in the appendix) such a choice may influence the speedup and convergence.

In the next section we present an exhaustive number of numerical tests executed on two distinct mas-

sively parallel clusters. We illustrate the limitation of the KSCG algorithm, compared to the ChASE eigensolver, and show how ChASE provides much better parallel scalability, which eventually will allow calculations on much more complex materials.

4. Numerical experiments

In this section we illustrate the results of a series of numerical experiments aimed at addressing the issues discussed above, related to matrix initialization and eigenproblem solutions using massively parallel computing clusters. We show how the restructuring of the parallel I/O dramatically reduces the time spent reading and setting up the BSE Hamiltonian matrix. We compare the KSCG and ChASE eigensolvers across a range of eigenproblems. Finally, we show how the use of ChASE enables our BSE code to further push the accessible physical parameter space, thanks to an enhanced use of parallel resources. The experiments are divided into three sets, each presenting a unique set up meant to drive our points home.

Strong scaling. We select a specific BSE eigenvalue problem, such that the size of its matrix fits into one computing node of a given cluster. We then initialize the matrix and solve for a small set of the eigenpairs using both ChASE and KSCG. This procedure is carried out for an increasing number of computing nodes to examine the scaling of the computation keeping the data set constant. On a log-log plot, a positive outcome would result in a linearly decreasing time-to-solution as a function of computing nodes used.

Weak scaling. For these experiments we successively increase the size of the BSE eigenvalue problem with the number of nodes, keeping the workload per compute node approximately constant. This is achieved by changing the energy cutoff E_{cut} of the BSE Hamiltonian. We compute the solutions of these eigenvalue problems with both KSCG and ChASE eigensolvers and examine the change in computing time. Good parallel behavior would result in a roughly constant time to solution as a function of the number of computing nodes.

Practical case: Converging the exciton-binding energy. In the last set of experiments, we showcase a study illustrating how leveraging a bigger set of computational resources enables us to solve very large BSE

matrices which were previously inaccessible. A typical example is provided by organic crystalline naphthalene, for which converging the exciton-binding energy with respect to the BSE energy cutoff E_{cut} requires solving matrices larger than previously considered. Thanks to the use of ChASE it was possible to reach the converged regime for the exciton-binding energy of this material.

Resources. Most of these experiments are performed on the National Science Foundation (NSF) BlueWaters supercomputer, hosted at the National Center for Supercomputing Applications (NCSA) at the University of Illinois, Urbana-Champaign. On BlueWaters we exclusively used the Cray “XE” compute nodes, each equipped with two AMD 6276 Interlagos processors connected via the Gemini interconnect. Each node has 16 floating point Bulldozer cores and 64 GB of memory. On BlueWaters our BSE code as well as the KSCG and ChASE eigensolvers are compiled with PGI v13.6.0 and linked against Cray’s LibSci v12.1.3, and MPICH v6.1.3.

We repeated a subset of the weak scaling tests on standard CPU and multi-GPU nodes of the JUWELS [49] cluster hosted at the Jülich Supercomputing Centre (JSC). Each standard node of JUWELS is equipped with two Dual Intel Xeon Platinum 8168 CPUs (48 cores), an EDR-Infiniband (Connect-X4) interconnect, and 96 GB of memory. In addition to standard compute nodes, JUWELS is equipped with 56 GPU nodes with two Dual Intel Xeon Gold 6148 CPUs (40 cores), connected via a dual EDR-Infiniband (Connect-X4) and 192 GB of memory each, hosting 4 NVIDIA V100 GPU cards. Currently, ChASE supports the use of a single GPU device per MPI rank. GPU experiments on JUWELS use all NVIDIA V100 by running 4 MPI processes per node. ChASE was compiled with the Intel compiler and Intel MKL version 19.0.3.199, ParaStation MPI version 5.2.2-1, and CUDA version 10.1.105. In the following, we explain these experiments in detail and analyze the results.

4.1. Strong scaling

For the strong scaling tests, we selected hafnium oxide, HfO_2 , with a Brillouin zone sampling of $6 \times 6 \times 6$ \mathbf{k} -points and a BSE energy cutoff of 9.1 eV. This corresponds to a BSE eigenvalue problem with a matrix size of $N = 41,252$, and we solve for the $m = 100$ lowest eigenpairs of the spectrum. In order to minimize overhead generated by MPI communicators, we

Table 1: Strong scaling and speedup of the code with the old I/O routine and KSCG solver, compared to the new parallel I/O implementation and the ChASE solver. Data is collected for runs using between 1 (16 threads) and 64 (1024 threads) processes.

# MPI ranks	Old I/O	Parallel I/O	Speedup	KSCG	ChASE	Speedup
1	336.55±6.10	791.16±19.69	0.43	5515.65±4.64	2390.08±2.59	2.31
4	374.96±9.08	374.26±7.21	1.00	1554.04±0.93	617.83±2.63	2.52
9	413.86±3.11	191.00±0.85	2.17	830.26±0.22	270.86±3.09	3.07
16	408.63±7.45	97.24±0.76	4.20	592.23±1.27	161.30±2.22	3.67
25	443.46±14.78	78.94±0.76	5.62	471.94±0.31	109.59±0.66	4.31
36	491.44±12.28	40.38±0.34	12.17	427.56±0.31	82.01±0.08	5.21
49	451.09±2.46	33.81±0.71	13.34	383.55±2.71	67.82±0.08	5.66
64	450.20±2.10	78.17±1.32	5.76	359.89±0.50	55.92±0.18	6.44

always use a number of MPI ranks which is the square of an integer number. This is due to the fact that most collective communications internal to ChASE are either AllReduce or Broadcasts which benefit from a square grid of processes; even better gain is achieved when the square is a power of two. We measured CPU time to completion within the BSE code for the tasks related to matrix initialization and eigenproblem solution, using between 1 and 64 processes³. For each node of BlueWaters (BW) we run the computation always with a number of threads equal to the total number of 16 floating point cores per node.

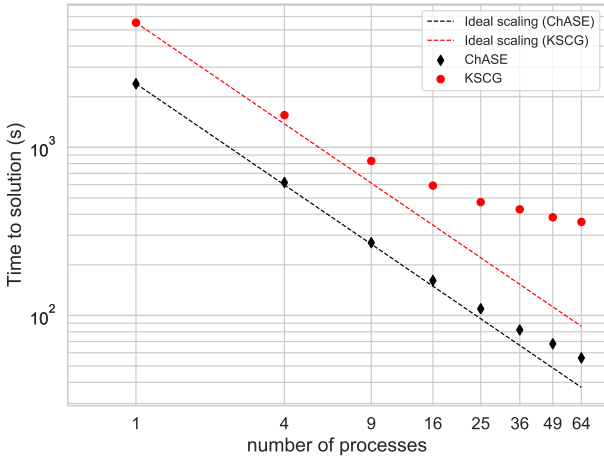


Figure 1: Strong scaling test. For a test with a specific number of MPI ranks, the computing time is averaged over 8 identical calculations on exactly the same computing nodes to account for statistical fluctuations in the floating point operations and communications among nodes.

We first show the benefit of adopting the new reading routine: Tab. 1 shows the improvement that

³We use equivalently and interchangeably the terms process and MPI rank.

the new parallel I/O delivers when compared to the original routine. In the original routine, only one MPI rank would read at a time, so while different ranks would read different files, only one rank would read at any given time. In practice, the code was no faster than having a single MPI rank read all files and broadcast the contents.

The new parallel routine scales well with increasing number of MPI ranks: For 1–4 MPI ranks, the CPU time of the new I/O is longer or comparable to the sequential routine, due to the additional “blocked” re-distribution process. While KSCG can use the old “stripped distribution”, this redistribution is needed when invoking ChASE. Beyond 4 MPI ranks, there is a stark improvement for the parallel routine and the peak speed-up of over 13 occurs for 49 MPI ranks for this example. The new algorithm is designed so that each MPI rank reads concurrently the part of the matrix that it holds, resulting in the lower half of the matrix being initialized. Subsequently the upper half is initialized by sending MPI one-to-one messages between the MPI ranks holding an initialized part of the matrix and the to-be-initialized transposed part. This approach avoids serialization during the I/O phase and only introduces a small amount of serialization among the ranks during the communication phase, reducing the time spent to read the complete matrix to barely more than the time required to read in the segment owned by any of the MPI ranks.

For the strong scaling experiment, and for both the KSCG and ChASE eigensolvers, we set the value $n_{ex} = 30$; this choice implies that the search space contains 30 additional eigenvalues on top of the wanted part of the spectra ($n_{ev} = 100$). This feature of subspace iteration eigensolvers is necessary in order to avoid that the convergence of the largest desired

eigenvectors becomes extremely slow. In order to demonstrate the scaling of the eigensolver, we show in Fig. 1 the time-to-solution as a function of the number of MPI ranks used. For each number of MPI ranks, the timings are averaged over 8 runs. Already on a single node, ChASE typically solves the eigenproblem in a fraction of the time needed by the KSCG solver. For the example chosen here, this corresponds to a 2.3x speed up, which grows to 6.4x on 64 nodes (see Tab. 1).

The growth in speedup, a consequence of the better scaling of the ChASE eigensolver, can be easily observed by comparing the deviation from the ideal scaling curves (dashed lines in Fig. 1); ChASE remains quite close to ideal scaling up to the largest number of compute nodes we used (64), but KSCG deviates from ideal scaling already for 16 nodes and is far off for 64 nodes. This behavior is expected, as the KSCG solver experiences an increase in the communication overhead relative to the time spent in carrying out actual computations. Thanks to the use of BLAS-3 kernels, ChASE makes better use of the CPU resources. Furthermore, it does not experience an early change of the ratio between computation and communication, until the amount of data per MPI rank starts becoming too small for the BLAS-3 kernels to take full advantage of their arithmetic intensity.

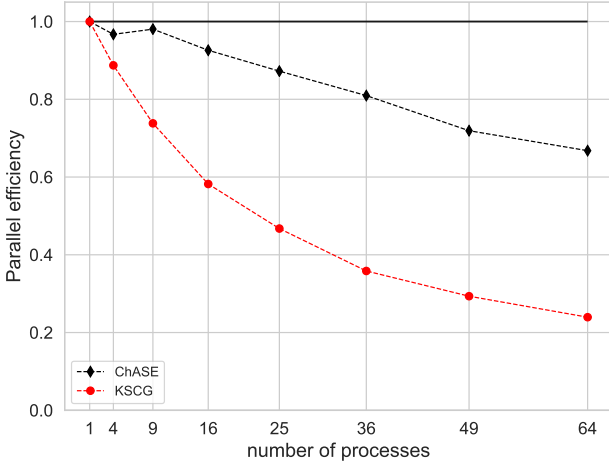


Figure 2: The parallel efficiency of the ChASE solver (black) and the CG solver (red) with respect to one compute node (16 cores).

This behavior is directly quantified by the parallel efficiency η of both solvers, which measures the loss in efficiency of a computational task as the number of

processing units p increases

$$\eta = \frac{t_{\text{ref}} * p_{\text{ref}}}{t * p}. \quad (2)$$

In our setup, the reference time t_{ref} and processing units p_{ref} refer to a single-node simulation with 16 cores. The plot of η versus the number of processes is shown in Fig. 2. It can be seen that the parallel efficiency of ChASE remains above 90 % up to 16 nodes, while that of the KSCG solver drops rather rapidly. For 64 ranks, the efficiency of the KSCG solver drops to 0.24, while that of the ChASE solver is still 0.67, well above the 50 % mark.

The speed up and parallel efficiency prove that the ChASE eigensolver significantly accelerates the process of obtaining solutions for practically relevant excitonic eigenvalue problems, and offers a better parallel behavior when compared to the KSCG solver. As mentioned in Sec. 3, the reason for the substantial speed up of ChASE comes from its use of highly optimized BLAS-3 computational kernels which extract as much performance as possible at the node level. The better scaling of ChASE resides in a lower communication overhead threshold which makes it more competitive.

4.2. Weak scaling

Weak scaling measures the behavior of a computational task when its workload is maintained constant while the computing resources are increased. In order to realize this set up we solve increasingly large eigenproblems, commensurate to the growth in number of compute nodes.

In this section, we illustrate the weak scaling of both eigensolvers using the Indium oxide (In_2O_3) system, that was previously studied in [32]. The \mathbf{k} -point sampling is fixed at $5 \times 5 \times 5$ and the BSE matrix size is changed through the BSE energy cutoff E_{cut} , which determines the number of non-interacting electron-hole pair states involved (see Sec. 2). Precisely tuning the energy cutoff allows us to adjust the matrix size from $N \sim 38,500$ to $N \sim 500,000$, while increasing the number of compute nodes and keeping the bulk of workload per node approximately constant. The matrix sizes corresponding to the different E_{cut} and the node counts are shown in Tab. 2.

Unfortunately, one cannot exactly predict the total workload to reach convergence for an iterative eigensolver, but it is reasonable to assume that its order of magnitude is $\mathcal{O}(N^2)$, as shown in Sec. 3.

Based on this assumption, the workload per node is kept within $\pm 0.5\%$ of that for the simulation on a single node. With this set of parameters, the utilization of the memory for each single node across different matrix sizes is kept at $\sim 80\%$ and $\sim 50\%$ in the BW cluster and JUWELS cluster, respectively.

The weak scaling tests executed on both clusters have slightly different goals: On BW we tested larger matrices with sizes up to half a million and compared the scaling between the KSCG and the ChASE solvers. On JUWELS we scanned a lower number of nodes and focused on just the ChASE eigensolver, executing it on CPU nodes and GPU equipped nodes. E_{cut} , the matrix size, and the number of MPI ranks are reported in Table 2 and we kept all other eigensolver parameters the same, i.e., $n_{\text{ev}}=100$ and $n_{\text{ex}}=25$. On BW we kept the number of MPI ranks the same as the number of nodes and set the number of OMP threads per rank equal to the total number of computing cores in each node. Because the JUWELS cluster has more cores per node and four GPU devices on each GPU node, we used 4 MPI ranks per node with 12 and 10 OMP threads per rank on the CPU nodes and GPU nodes, respectively.

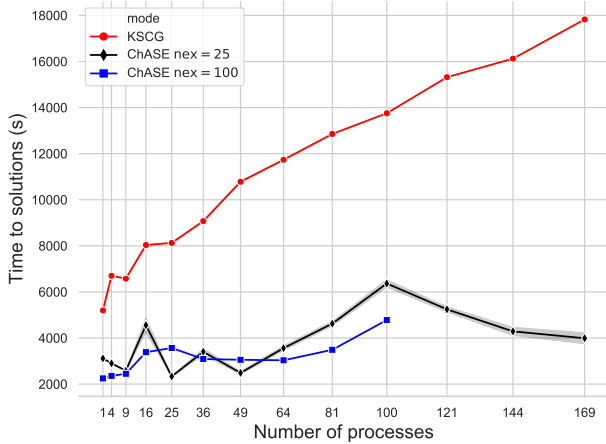


Figure 3: Weak scaling test. Averages over 5 runs are performed for ChASE with $n_{\text{ex}} = 25$ and the error bars are plotted.

Figure 3 illustrates weak scaling of ChASE and KSCG via the total time needed to solve for the first 100 eigenpairs as a function of the number of computing nodes used on BW. In order to determine variability, we executed this test on BW 5 times for each of the distinct matrix sizes and solvers and averaged over the measured completion times. While for ChASE this procedure was repeated for all node configura-

tions, for the KSCG solver this average is only performed up to 81 nodes due to the high computational cost and the small standard deviation. Since the KSCG error bars were no larger than 0.2% across all calculations and are not visible in the plot, only ChASE standard deviation is shown. We also repeated the numerical tests for ChASE with a different value of $n_{\text{ex}}=100$ and discuss motivation and results in Sec. 4.3.

Figure 3 shows that for KSCG the increase in time is almost monotonic and for ChASE it follows an oscillating behavior as the number of processes increases. For the KSCG solver, the maximum time of execution (17,825 secs on 169 nodes) is about 3.4 times longer than the minimum (5,197 secs on a single node). Correspondingly, the longest time of execution (6,522 secs on 100 nodes) for ChASE is only 2.67 times longer than the shortest time (2,443 secs on 25 nodes), indicating a better weak scaling of the ChASE solver. While the smallest and largest time-to-solution for both solvers occur for different node counts, it is important to notice that the ratio between the minima and maxima of the two solvers increases from 2.1 to 2.7. This increasing trend is analogous to the increase in speed-up between the two solvers in the strong scaling case, indicating a better parallel efficiency for the ChASE eigensolver. This trend is even more evident for node counts above 100 nodes: the speed up of ChASE with respect to KSCG keeps increasing consistently, reaching 4.3 at 169 nodes.

The timing for ChASE varies especially in the range between 16 and 64 nodes, corresponding to matrix sizes between 10^5 and 3×10^5 . These oscillations are in part algorithmic and in part due to variation in the communication overhead. The algorithmic causes of oscillations originate in the iterative nature of the ChASE solver. Because iterative numerical algorithms are not deterministic, they do not have a constant work per byte of data. In other words, one cannot predict a-priori the number of operations necessary to reach a solution. In the specific case of ChASE, what varies is 1) the number of subspace iterations, and 2) the different counts of matrix-vector operations required to converge across eigenproblems of different size (see supplementary material for more details). Both these factors directly determine the effective workload associated with an eigenproblem solution by ChASE.

The communication overhead is mostly due to two MPI collectives used in the ChASE implementation:

Table 2: E_{cut} and matrix sizes used for the weak scaling tests on the Blue Waters and JUWELS clusters as a function of the computing nodes.

nodes	Blue Waters		JUWELS			Energy cutoff (eV)	Matrix size (N)
	MPI	OMP	MPI	OMP(CPU)	OMP(GPU)		
1	1	16	4	48	40	6.45	38,537
4	4	64	16	192	160	7.45	76,887
9	9	144	36	432	360	8.31	115,459
16	16	256	64	768	640	9.11	154,023
25	25	400	100	1200	1000	9.87	192,788
36	36	576	144	1728	1440	10.54	231,011
49	49	784	196	2352	1960	11.15	269,645
64	64	1024				11.73	307,865
81	81	1296				12.30	346,915
100	100	1600				12.82	385,183
121	121	1936				13.32	423,607
144	144	2304				13.83	462,469
169	169	2704				14.30	500,649

AllReduce and Broadcast. We illustrate their effect in more detail later in this section when discussing experiments executed on JUWELS. In conclusion, the numerical behavior of KSCG and ChASE is influenced by similar factors having different effects on both solvers. Time spent in inter-node communication tends to increase timings for both solvers as the number of computing nodes grows. The less regular behavior of ChASE is additionally determined by the changes in the effective workload executed by the solver.

The results of the tests executed on the JUWELS cluster [49] are shown in Fig. 4. The parameters of ChASE execution were the same as for Blue Waters, namely $\text{nev}=100$ and $\text{nex}=25$. To match the number of GPU devices hosted by JUWELS GPU nodes, we use a different configuration of the computing resources by assigning four MPI ranks to each node. In order to improve the statistical analysis of our results we executed 15 repetitions for any given matrix size on both CPU and GPU nodes. For each point in the plot we show the average and its 95% confidence interval (CI) based on the standard deviation. The results are shown as a set of points, blue indicating time-to-solution for the CPU nodes and green for the GPU nodes, encased by a shaded area indicating the CI.

While the standard deviation for CPU nodes is much larger than for GPU nodes, the time-to-solution on CPU nodes and GPU nodes also shows noticeable

similarities of the pattern of variation as a function of the number of processes. In particular, a big jump can be observed in going from 16 to 36 processes. This is a typical case where there are two factors both adding to the computing time: a drastic increase in the total matrix-vector operations executed by ChASE and a substantial increase in latency of the many calls to MPI AllReduce. We have benchmarked such call (as well as the Ibcast call) and observed a jump from 15.6 ms to 21.9 ms in average latency. Likewise, ChASE performs 8,160 and 11,360 matrix-vector multiplications using 16 and 36 MPI ranks, respectively (see complete set of data in the supplementary material). This latter effect is not always positive but it may also favor a decrease in run time as it can be deduced observing that the number of matrix-vector operation decreases from 11,360 to 9,340 in going from 36 to 100 MPI ranks, respectively. On top of these two effects, the average latency of MPI Bcast keeps increasing, contributing with a constant ratio to the overall increase in time-to-solution.

Overall, it is clear that, whenever possible, an execution over multiple GPU devices should be preferred, since in the worst-case scenario it halves the run time with respect to the use of only CPU nodes. On the other hand, the peak performance of the four NVIDIA V100 GPUs is significantly larger than two times that of the CPU nodes, which implies that the use of the GPUs is not as efficient as on the multi-cores. This effect is expected since cuBLAS is less efficient than the

Multi-threaded MKL BLAS in dealing with repeated multiplications between a square and a tall and skinny matrix. In addition, there is some unavoidable overhead due to the transfer of the filtered vectors from the main to the local GPU memory and vice versa.

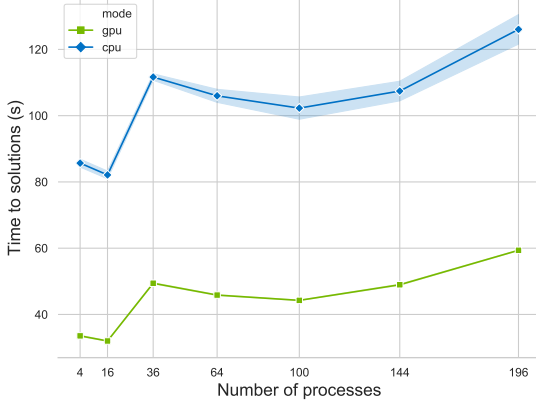


Figure 4: Plot of weak scaling results for the ChASE solver on JUWELS for both CPU (blue) and GPU (green) nodes. Statistics are over 15 runs. The plot shows average and 95 % confidence interval based on standard deviation in shade of the same color.

4.3. Search space and ChASE convergence

As shown in Ref. [9], the convergence of ChASE can be significantly affected by the choice of the number of additional eigenpairs n_{ex} , which together with the wanted part of the spectra form the full search space. Specifically, in ChASE the convergence of a given eigenpair (λ_a, x_a) is deterministic and is related to the distance between λ_a and the center of the interval $[\lambda_{\text{nev}+n_{\text{ex}}}, \lambda_{\text{max}}]$ divided by its half-width. In our weak-scaling test the minimum eigenvalue λ_1 changes very little, while the maximum eigenvalue λ_{max} gets significantly larger as the size of the matrices increases. In turn, such a change leads to a worsening of the convergence ratios of the desired eigenpairs (see example for the correlation between the convergence of the solver and the matrix size in the supplemental information). The convergence can be improved by increasing the n_{ex} value such that $\lambda_{\text{nev}+n_{\text{ex}}}$ is increased accordingly. However, as more extra eigenvalues are added, the convergence of the iterative solver is improved at the expense of increasing the workload due to a larger number of the vectors that iterate and need to be filtered. In an attempt to obtain a less oscillatory curve for the weak scaling for ChASE on BW, we now analyze how the behavior of the solver

can be influenced by the n_{ex} value as the matrix size increases.

To illustrate the effect of the n_{ex} value, we measured the time-to-solution for the same weak scaling problem set, but with $n_{\text{ex}} = 100$. In Fig. 3 we compare these results up to 100 nodes and observe that increasing n_{ex} leads to a more flat curve of the time-to-solution for ChASE. Between 9 and 64 nodes it can be clearly seen that the run time oscillates less, compared to $n_{\text{ex}} = 25$. In addition, the three largest matrices benefit substantially from choosing a larger n_{ex} showing a consistent decrease in timing. Intermediate size matrices do not benefit in the same way. As mentioned above, this is attributed to the trade-off between two competing factors; the performance gain obtained from a better convergence rate and the increased in size of the search space which causes a growth in workload.

To prove this point, we picked the matrix of size $N = 231,011$ and measured the run time as a function of n_{ex} . Indeed we observe an optimized value of n_{ex} around 40–50 (see details in the supplemental information). A potential way to improve the choice of n_{ex} across different matrices is to perform such a test once, and then predict the n_{ex} value accordingly across different matrix sizes. Predicting a scaling factor in a systematic way, however, is not straightforward, and can be affected significantly by the distribution of eigenvalues in the overall spectra. Thus, it can depend significantly on the number of desired eigenpairs.

4.4. A practical case: converging exciton-binding energy in naphthalene

In this section, we illustrate how the adoption of ChASE enables us to address physical problems which were inaccessible before, due to their high computational cost. In particular, we show that using ChASE enables to solve for extremely large eigenvalue problems that occur when accurately converging the exciton binding energy of a crystal with respect to the BSE energy cutoff. Here we use the example of a naphthalene organic crystal (see Fig. 5 for the crystal structure of the material): In this system, the exciton-binding energy converges slowly with respect to the BSE energy cutoff and requires matrices with ranks up to $\sim 500,000$. This is only possible thanks to the excellent weak scaling behavior of the ChASE eigen-solver.

Table 3: BSE matrices for the convergence test of the exciton binding energy (in eV) for a naphthalene organic crystal with respect to the BSE energy cutoff (in eV). As the size increases (with increasing energy cutoff) we use more processes with the ChASE solver. Compute timings (in s) and the binding energies of the dark and optically active excitonic state are reported (see text).

$1/E_{\text{cut}}$	size	# processes	time (s)	$E_{\text{b, dark}}$	$E_{\text{b, active}}$
0.1667	7172	16	10.672	1.18224	0.93402
0.125	22264	16	69.087	1.2053	0.97823
0.1	49888	36	176.678	1.23005	1.03827
0.0833	92220	36	626.752	1.23496	1.06192
0.0714	149808	36	2829.956	1.23945	1.09635
0.0625	217292	36	3316.959	1.24473	1.13995
0.0556	296648	64	3882.796	1.24878	1.1908
0.05	381364	121	4443.877	1.25251	1.23184
0.0455	472444	169	4256.253	1.25671	1.26287

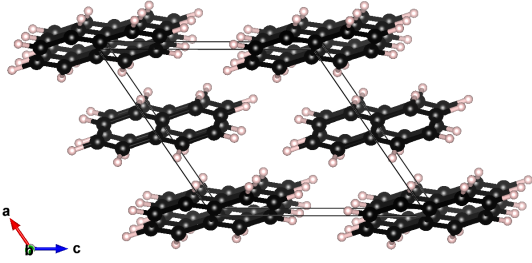


Figure 5: Primitive unit cell of naphthalene crystal with black spheres being carbon atoms and white spheres being hydrogen atoms. a , b , and c labels the crystal axis.

Naphthalene is an organic crystal with 20 carbon atoms and 16 hydrogen atoms per primitive unit cell. We treat carbon $2s$ and carbon $2p$ as valence electrons, leading to a total of 96 valence electrons. Although this unit cell is not as large as that for In_2O_3 , there are noteworthy difficulties in obtaining exciton-binding energies: The lowest three bound excitonic states are dark, which means that their optical oscillator strength, representing the strength of the dipole transition, is low. In practice, the exciton binding energy in this material is typically defined as the difference between the lowest peak of the imaginary part of the dielectric function without and with considering excitonic effects [50]. The lowest peak with excitonic effects included corresponds to the fourth lowest eigenvalue of the BSE matrix. Thus, we study the convergence of both optically dark and active states with respect to BSE energy cutoff in this work.

To this end, we compute the lowest eigenvalue (dark excitonic state) and the fourth-lowest eigenvalue (optically active excitonic state of the first peak for light polarization along the y direction). We re-

port the size of the eigenproblem, the run time for ChASE, and the calculated exciton binding energies in Tab. 3. It can be seen from the table that as the energy cutoff increases (decreasing $1/E_{\text{cut}}$), the matrix size increases significantly and reaches $\sim 500,000$ for the largest energy cutoff we simulated. Using the KSCG solver, it was not possible to tackle matrices of this size, and the largest matrix that we can reach was on the order of $\sim 200,000$, corresponding to $E_{\text{cut}} = 16$ eV.

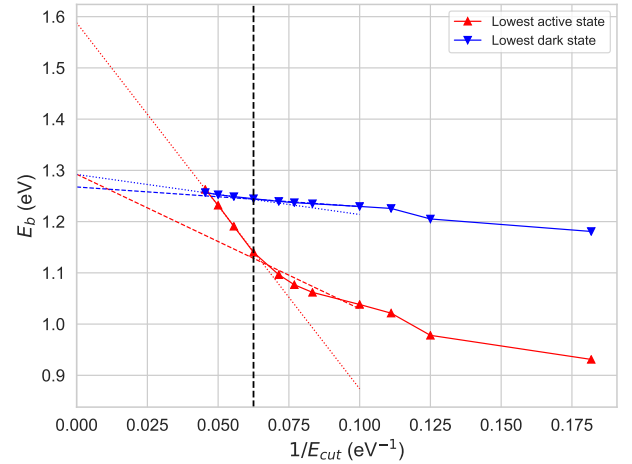


Figure 6: Convergence of the exciton-binding energy of the lowest dark state (blue) and first optically active state (red) with respect to the BSE energy cutoff E_{cut} . Extrapolation of the curve to zero results in the exciton binding energy and is shown using data points from $E_{\text{cut}}=10-16$ eV (dashed line, red and blue) and $E_{\text{cut}}=18-22$ eV (dotted line, red and blue). The black dashed vertical line represents the limit of KSCG solver.

The convergence test in Fig. 6 shows that by pushing the matrix size beyond what was possible using the KSCG solver, we find a great improvement of the

convergence of exciton-binding energy for this material. As mentioned in Sec. 2, the converged exciton-binding energy is obtained through linear extrapolation of the corresponding eigenvalues of matrices computed using the largest values of E_{cut} . In particular, we compare extrapolations of E_b obtained using data points from $E_{\text{cut}}=10-16$ eV (achievable using the KSCG solver), and from $E_{\text{cut}}=18-22$ eV (only achievable using the ChASE library).

This figure shows that for both the dark and the optically active state, the linear regime starts emerging only after matrix sizes $N \sim 200,000$, corresponding to $E_{\text{cut}} = 16$ eV. Significant differences can be seen between the extrapolation results using the two sets of data. For the dark state, using only data points in the range of $E_{\text{cut}} = 10-16$ eV results in an extrapolated value of $E_b = 1.267$ eV, compared to a value of $E_b = 1.292$ eV obtained using data points in the range $E_{\text{cut}}=18-22$ eV. The difference is much larger for the optically active state, with the extrapolation of $E_b = 1.293$ eV ($E_{\text{cut}} = 10-16$ eV) vs. $E_b = 1.588$ eV ($E_{\text{cut}} = 18-22$ eV). In other words, using eigenvalues exclusively computed with the KSCG algorithm underestimates the value of the extrapolated exciton binding energy by 2 % and 18.6 %, for the lowest dark and lowest active state, respectively. The underestimation of the exciton-binding energy for the lowest active state is not only large, but also plays a more important role from a practical point of view. The lowest optically active state corresponds to the onset of measurable optical absorption and impacts the use of a material, e.g. for optoelectronic applications, more than the lowest dark state. Many similar materials exhibit optically dark lowest excitonic states and the lowest optically active states higher in energy [51, 52].

In summary, using naphthalene as an example, we show that increasing the size of the BSE Hamiltonian is critical to obtain an accurate extrapolation of the exciton-binding energy. Integrating the ChASE solver into our code allows us to solve eigenproblems with matrix sizes two to five times larger than what was possible before. Adoption of the ChASE solver, thus, enables more accurate predictions of the exciton-binding energy and opens up opportunities to study the optical properties of materials more accurately. This can benefit many applications such as organic solar cells, for which knowledge of the exciton binding energy is amongst the most important aspects to be uncovered [52].

5. Summary and Conclusions

We described and analyzed the modernization of a legacy theoretical spectroscopy code. This code allows for *in silico* predictions of optoelectronic properties of materials by solving the Bethe-Salpeter equation for the optical polarization function. Here we identified two main bottlenecks, namely the initialization of the underlying excitonic Hamiltonian matrix from disk and the solution of the corresponding eigenvalue problem for a small fraction of the lowest part of the spectrum. We addressed each bottleneck individually: First we re-factor and parallelize the I/O routines that are responsible for reading the matrix elements from files and distributing them among the compute nodes. Second, we integrate the scientific software ChASE, a new parallel library specialized in solving for partial spectra of large and dense Hermitian eigenproblems.

Our results show that the new parallel I/O routine scales well with the number of compute nodes and in our test we find a speed-up of up to 13.34 compared to the legacy implementation. This was determined when reading a matrix of size 41,252 on 49 compute nodes, i.e., a total of about 842 rows per MPI rank, below which increasing inter-node communication reduces the speedup.

To characterize the implementation of ChASE for finding the lowest eigenvalues, we carry out three sets of performance measurements: Strong scaling tests, weak scaling tests, and tests on the convergence of the excitonic binding energy of organic crystalline naphthalene. The last set of tests illustrates for a material of practical importance that the modernized code can access exciton physics at a scale that was previously unattainable. Using these results we demonstrate that the integration of the new ChASE library into the BSE code achieves two main objectives: First it enhances both the parallelism and the scaling behavior of the scientific software, allowing it to be used on the current and future parallel clusters. Second, it extends the ability of the software to tackle scientific questions which could not be answered so far with the necessary accuracy.

This is a success story of how to modernize a code by changing both its algorithmic structure and the middleware embedded in it. Because the significantly higher computational cost of the previous implementation imposed accuracy limitations, it became a necessity to reduce such costs by addressing the existing

bottlenecks. The end result is a rejuvenated BSE code that will allow its users to study novel problems at scales inaccessible before. Overall, the modernization of this scientific software has extended its lifetime especially in light of current computing cluster moving towards the exascale target.

This work describes the results of a long term project initiated under the Joint Laboratory for Extreme Scale Computing (JLESC), an international consortia of Supercomputing Centers and Research institutions. The interdisciplinary nature of the challenge at the core of this project brought together researchers from diverse fields as condensed matter physics, numerical linear algebra, and high-performance computing across two continents. The results obtained are a demonstration how effective is a multi-disciplinary team in addressing a computational challenge that requires a variety of expertise.

Acknowledgments

This material is based upon work supported by the National Science Foundation under Grant No. DMR-1555153. This research is part of the Blue Waters sustained-petascale computing project, which is supported by the National Science Foundation (awards OCI-0725070 and ACI-1238993) and the state of Illinois. Blue Waters is a joint effort of the University of Illinois at Urbana-Champaign and its National Center for Supercomputing Applications. The authors acknowledge the computing time granted through Jülich Supercomputing Centre on the supercomputer JUWELS at Forschungszentrum Jülich. Financial support from the Deutsche Forschungsgemeinschaft (DFG) through grant GSC 111 is also gratefully acknowledged. This research is partially supported by the NCSA-Inria-ANL-BSC-JSC-Riken-UTK Joint-Laboratory for Extreme Scale Computing (JLESC, <https://jlesc.github.io/>), which enabled joint workshop attendance for scientific discussions and a visit of E. D. N. and J. W. at NCSA in Urbana-Champaign.

References

- [1] H. Anzt, E. Boman, R. Falgout, P. Ghysels, M. Heroux, X. Li, L. Curfman McInnes, R. Tran Mills, S. Rajamanickam, K. Rupp, B. Smith, I. Yamazaki, U. Meier Yang, Preparing sparse solvers for exascale computing, *Philosophical Transactions of the Royal Society A: Mathematical, Physical and Engineering Sciences* 378 (2166) (2020) 20190053. doi:10.1098/rsta.2019.0053.
- [2] D. E. Bernholdt, S. Boehm, G. Bosilca, M. Gorenla Venkata, R. E. Grant, T. Naughton, H. P. Pritchard, M. Schulz, G. R. Vallee, A survey of mpi usage in the us exascale computing project, *Concurrency and Computation: Practice and Experience* 32 (3) (2020) e4851, e4851 cpe.4851. doi:10.1002/cpe.4851.
- [3] D. Kothe, S. Lee, I. Qualters, Exascale computing in the united states, *Computing in Science Engineering* 21 (1) (2019) 17–29. doi:10.1109/MCSE.2018.2875366.
- [4] M. Shao, F. da Jornada, L. Lin, C. Yang, J. Deslippe, S. Louie, A structure preserving lanczos algorithm for computing the optical absorption spectrum, *SIAM Journal on Matrix Analysis and Applications* 39 (2) (2018) 683–711. doi:10.1137/16M1102641.
- [5] F. Fuchs, C. Rödl, A. Schleife, F. Bechstedt, Efficient $\mathcal{O}(N^2)$ approach to solve the bethe-salpeter equation for excitonic bound states, *Phys. Rev. B* 78 (2008) 085103. doi:10.1103/PhysRevB.78.085103. URL <https://link.aps.org/doi/10.1103/PhysRevB.78.085103>
- [6] C. Rödl, F. Fuchs, J. Furthmüller, F. Bechstedt, Ab initio theory of excitons and optical properties for spin-polarized systems: Application to antiferromagnetic MnO, *Phys. Rev. B* 77 (2008) 184408.
- [7] E. E. Salpeter, H. A. Bethe, A relativistic equation for bound-state problems, *Phys. Rev.* 84 (6) (1951) 1232. doi:10.1103/PhysRev.84.1232.
- [8] G. Onida, L. Reining, A. Rubio, Electronic excitations: density-functional versus many-body green’s-function approaches, *Rev. Mod. Phys.* 74 (2) (2002) 601. doi:10.1103/RevModPhys.74.601.
- [9] J. Winkelmann, P. Springer, E. D. Napoli, ChASE: Chebyshev Accelerated Subspace iteration Eigensolver for sequences of Hermitian eigenvalue problems, *ACM Trans. Math. Softw.* 45 (2) (2019) 21. doi:10.1145/3313828.
- [10] A. Miyata, A. Mitoglu, P. Plochocka, O. Portugall, J. T. Wang, S. D. Stranks, H. J. Snaith, R. J. Nicholas, Direct measurement of the exciton binding energy and effective masses for charge carriers in organic-inorganic tri-halide perovskites, *Nat. Phys.* 11 (7) (2015) 582–587.
- [11] C. Klingshirn, ZnO: material, physics and applications, *ChemPhysChem* 8 (6) (2007) 782–803.
- [12] P. Drude, Ueber die gesetze der reflexion und brechung des lichtes an der grenze absorbirender krystalle, *Ann. Phys. (Berl.)* 268 (12) (1887) 584–625. doi:10.1002/andp.18872681205.
- [13] S. Perkowitz, Optical characterization of semiconductors: infrared, Raman, and photoluminescence spectroscopy, Vol. 14, Elsevier, 2012.
- [14] S. Hüfner, Photoelectron spectroscopy: principles and applications, Springer Science & Business Media, 2013.
- [15] M. P. Ljungberg, P. Koval, F. Ferrari, D. Foerster, D. Sánchez-Portal, Cubic-scaling iterative solution of the bethe-salpeter equation for finite systems, *Phys. Rev. B* 92 (2015) 075422. doi:10.1103/PhysRevB.92.075422.
- [16] L. S. Blackford, J. Choi, A. Cleary, E. D’Azevedo, J. Demmel, I. Dhillon, J. Dongarra, S. Hammarling, G. Henry, A. Petitet, K. Stanley, D. Walker, R. C. Whaley, ScaLAPACK Users’ Guide, SIAM, Philadelphia, PA, 1997. doi:10.1137/1.9780898719642.
- [17] J. Kurzak, P. Wu, M. Gates, I. Yamazaki, P. Luszczek, G. Ragghianti, J. Dongarra, Designing SLATE: Software

- for Linear Algebra Targeting Exascale, Tech. rep., University of Tennessee (10 2017).
- [18] M. Geradin, The computational efficiency of a new minimization algorithm for eigenvalue analysis, *J. Sound Vib.* 19 (1971) 319.
 - [19] I. Fried, Optimal gradient minimization scheme for finite element eigenproblems, *J. Sound Vib.* 20 (1972) 333.
 - [20] J. K. Cullum, R. A. Willoughby, *Lanczos Algorithms for Large Symmetric Eigenvalue Computations Volume 1, Theory*, Birkhauser, 1985.
 - [21] V. Hernandez, J. E. Roman, V. Vidal, SLEPc: A Scalable and Flexible Toolkit for the Solution of Eigenvalue Problems, *ACM Transactions on Mathematical Software* 31 (3) (2005) 351–362. doi:10.1145/1089014.1089019. URL <http://doi.acm.org/10.1145/1089014.1089019>
 - [22] M. A. Heroux, R. A. Bartlett, V. E. Howle, R. J. Hoekstra, J. J. Hu, T. G. Kolda, R. B. Lehoucq, K. R. Long, R. P. Pawlowski, E. T. Phipps, A. G. Salinger, H. K. Thornquist, R. S. Tuminaro, J. M. Willenbring, A. Williams, K. S. Stanley, An Overview of the Trilinos Project, *ACM Transactions on Mathematical Software* 31 (3) (2005) 397–423. doi:10.1145/1089014.1089021. URL <http://doi.acm.org/10.1145/1089014.1089021>
 - [23] P. H. Hahn, W. G. Schmidt, F. Bechstedt, Bulk excitonic effects in surface optical spectra, *Phys. Rev. Lett.* 88 (2001) 016402. doi:10.1103/PhysRevLett.88.016402.
 - [24] W. G. Schmidt, S. Glutsch, P. H. Hahn, F. Bechstedt, Efficient $\mathcal{O}(N^2)$ method to solve the bethe-salpeter equation, *Phys. Rev. B* 67 (2003) 085307. doi:10.1103/PhysRevB.67.085307.
 - [25] L. Hedin, New Method for Calculating the One-Particle Green’s Function with Application to the Electron-Gas Problem, *Phys. Rev.* 139 (1965) A796–A823. doi:10.1103/PhysRev.139.A796.
 - [26] S. Louie, Predicting materials and properties: Theory of the ground and excited state, in: S. G. Louie, M. L. Cohen (Eds.), *Conceptual Foundations of Materials*, Vol. 2 of Contemporary Concepts of Condensed Matter Science, Elsevier, 2006, Ch. 2, pp. 9–53. doi:10.1016/S1572-0934(06)02002-6.
 - [27] F. Bechstedt, Many-Body Approach to Electronic Excitations, Vol. 181 of Springer Series in Solid-State Sciences, Springer-Verlag Berlin Heidelberg, 2015. doi:10.1007/978-3-662-44593-8.
 - [28] P. Hohenberg, W. Kohn, Inhomogeneous Electron Gas, *Physical Review* 136 (1964) B864–B871. doi:10.1103/PhysRev.136.B864.
 - [29] W. Kohn, L. J. Sham, Self-consistent equations including exchange and correlation effects, *Phys. Rev.* 140 (1965) A1133–A1138. doi:10.1103/PhysRev.140.A1133.
 - [30] A. Seidl, A. Görling, P. Vogl, J. A. Majewski, M. Levy, Generalized kohn-sham schemes and the band-gap problem, *Phys. Rev. B* 53 (1996) 3764–3774. doi:10.1103/PhysRevB.53.3764.
 - [31] A. Schleife, C. Rödl, F. Fuchs, J. Furthmüller, F. Bechstedt, Optical and energy-loss spectra of mgo, zno, and cdo from ab initio many-body calculations, *Phys. Rev. B* 80 (3) (2009) 035112.
 - [32] A. Schleife, M. D. Neumann, N. Esser, Z. Galazka, A. Gottwald, J. Nixdorf, R. Goldhahn, M. Feneberg, Optical properties of in2o3 from experiment and first-principles theory: influence of lattice screening, *New J. Phys.* 20 (5) (2018) 053016.
 - [33] X. Zhang, A. Schleife, Nonequilibrium bn-zno: Optical properties and excitonic effects from first principles, *Phys. Rev. B* 97 (2018) 125201. doi:10.1103/PhysRevB.97.125201. URL <https://link.aps.org/doi/10.1103/PhysRevB.97.125201>
 - [34] I. S. Dhillon, B. N. Parlett, Multiple representations to compute orthogonal eigenvectors of symmetric tridiagonal matrices, *Linear Algebra and its Applications* 387 (2004) 1–28.
 - [35] P. Bientinesi, I. S. Dhillon, R. A. van de Geijn, A Parallel Eigensolver for Dense Symmetric Matrices Based on Multiple Relatively Robust Representations, *J. Scientific Computing* 27 (1) (2005) 43–66. doi:10.1137/030601107.
 - [36] T. Kalkreuter, H. Simma, An accelerated conjugate gradient algorithm to compute low-lying eigenvalues? a study for the dirac operator in su (2) lattice qcd, *Comput. Phys. Commun.* 93 (1) (1996) 33–47.
 - [37] G. Kresse, J. Hafner, Ab initio molecular dynamics for liquid metals, *Phys. Rev. B* 47 (1993) 558–561. doi:10.1103/PhysRevB.47.558. URL <https://link.aps.org/doi/10.1103/PhysRevB.47.558>
 - [38] G. Kresse, J. Furthmüller, Efficiency of ab-initio total energy calculations for metals and semiconductors using a plane-wave basis set, *Computational Materials Science* 6 (1) (1996) 15 – 50. doi:https://doi.org/10.1016/0927-0256(96)00008-0. URL <http://www.sciencedirect.com/science/article/pii/0927025696000080>
 - [39] G. Kresse, J. Furthmüller, Efficient iterative schemes for ab initio total-energy calculations using a plane-wave basis set, *Phys. Rev. B* 54 (1996) 11169–11186. doi:10.1103/PhysRevB.54.11169. URL <https://link.aps.org/doi/10.1103/PhysRevB.54.11169>
 - [40] D. S. Watkins, *The Matrix Eigenvalue Problem: GR and Krylov Subspace Methods*, 1st Edition, Society for Industrial and Applied Mathematics, USA, 2007.
 - [41] A. Schleife, F. Bechstedt, Ab initio description of quasi-particle band structures and optical near-edge absorption of transparent conducting oxides, *J. Mater. Res.* 27 (17) (2012) 2180–2189.
 - [42] K. Kang, A. Kononov, C.-W. Lee, J. A. Leveillee, E. P. Shapera, X. Zhang, A. Schleife, Pushing the frontiers of modeling excited electronic states and dynamics to accelerate materials engineering and design, *Comput. Mater. Sci.* 160 (2019) 207–216. doi:10.1016/j.commatsci.2019.01.004.
 - [43] T. Imamura, S. Yamada, M. Machida, Development of a High Performance Eigensolver on the Petascale next Generation Supercomputer System, *Progress in Nuclear Science and Technology* 2 (2011) 643–650. doi:10.15669/pnst.2.643.
 - [44] A. Marek, V. Blum, R. Johanni, V. Havu, B. Lang, T. Auckenthaler, A. Heinecke, H.-J. Bungartz, H. Lederer, The ELPA library: Scalable Parallel Eigenvalue Solutions for Electronic Structure Theory and Computational Science, *Journal of Physics: Condensed Matter* 26 (21) (2014) 213201. doi:10.1088/0953-8984/26/21/213201.
 - [45] W. zhe Yu Victor, C. Campos, W. Dawson, A. García,

- V. Havu, B. Hourahine, W. P. Huhn, M. Jacquelin, W. Jia, M. Keceli, R. Laasner, Y. Li, L. Lin, J. Lu, J. Moussa, J. E. Roman, A. Vázquez-Mayagoitia, C. Yang, V. Blum, ELSI – An Open Infrastructure for Electronic Structure Solvers, arXiv:1912.13403, arXiv preprint (12 2019).
- [46] K. Goto, R. A. v. d. Geijn, Anatomy of high-performance matrix multiplication, *ACM Trans. Math. Softw.* 34 (3) (2008) 1–25. doi:10.1145/1356052.1356053.
URL <http://portal.acm.org/citation.cfm?doid=1356052.1356053>
- [47] K. Goto, R. van de Geijn, High-performance implementation of the level-3 BLAS, *ACM Transactions on Mathematical Software* 35 (1) (2008) 1–14.
- [48] J. Huang, L. Rice, D. A. Matthews, R. A. v. d. Geijn, Generating Families of Practical Fast Matrix Multiplication Algorithms, in: 2017 IEEE International Parallel and Distributed Processing Symposium (IPDPS), IEEE, Orlando, FL, USA, 2017, pp. 656–667. doi:10.1109/IPDPS.2017.56.
URL <http://ieeexplore.ieee.org/document/7967156/>
- [49] Jülich Supercomputing Centre, JUWELS: Modular Tier-0/1 Supercomputer at the Jülich Supercomputing Centre, *Journal of large-scale research facilities* 5 (A135) (2019). doi:10.17815/jlsrf-5-171.
URL <http://dx.doi.org/10.17815/jlsrf-5-171>
- [50] K. Hummer, C. Ambrosch-Draxl, Oligoacene exciton binding energies: Their dependence on molecular size, *Phys. Rev. B* 71 (2005) 081202. doi:10.1103/PhysRevB.71.081202.
- [51] H. Takagi, H. Kunugita, K. Ema, Influence of the image charge effect on excitonic energy structure in organic-inorganic multiple quantum well crystals, *Phys. Rev. B* 87 (2013) 125421. doi:10.1103/PhysRevB.87.125421.
URL <https://link.aps.org/doi/10.1103/PhysRevB.87.125421>
- [52] D. N. Congreve, J. Lee, N. J. Thompson, E. Hontz, S. R. Yost, P. D. Reusswig, M. E. Bahlke, S. Reineke, T. Van Voorhis, M. A. Baldo, External quantum efficiency above 100% in a singlet-exciton-fission-based organic photovoltaic cell, *Science* 340 (6130) (2013) 334–337. doi:10.1126/science.1232994.
- [53] J. Liu, B. Chandrasekaran, W. Yu, J. Wu, D. Buntinas, S. Kini, D. K. Panda, P. Wyckoff, Microbenchmark performance comparison of high-speed cluster interconnects, *Ieee Micro* 24 (1) (2004) 42–51.

S1. Supplemental materials

In this section we report on additional data relative to the numerical tests described and discussed in Sec. 4. Most of the data is presented in table formats with few additional comments on the data format and its significance.

S1.1. Strong scaling tests

Table S1 and Table S2 report the full timings recorded for the ChASE and the CG solver, respectively. The timing is broken into multiple main parts:

- **Pre-reading:** Before reading any matrices or actual data, these indicate the task of reading the input parameters, initialization, or allocations, these are collected in one single timer.
- **Read optics:** After the initialization, the optical transition matrix elements, as well as the DFT energies are read from the ground state calculation of the material system.
- **Reading and building:** This label indicates the task of proper reading and initializing the BSE matrix. In the paper we have used the term I/O for this task. This is the first bottleneck for which the code was modernized and where we observe substantial improvement with respect to the old code.
- **CG/ChASE:** This label corresponds to the time spent in obtaining the lowest set of eigenpairs of the BSE Hamiltonian either using the Conjugate gradient solver or ChASE library. This is the second and most substantial bottleneck of the BSE code and where we observe a marked difference with respect to the old code.
- **Total:** This label indicates the sum of all timings above.

Table S1: Strong scalability test of the code with new reading routine and ChASE solver. For all different runs, 16 threads are used per MPI rank and the data is averaged over 8 runs on the same node(s)

# MPI ranks	Pre-reading	Read optics	Reading/Building	ChASE	Total
1	26.26±0.04	26.29±0.01	791.16±19.69	2390.08±2.59	3235.15±19.43
4	29.91±0.13	30.03±0.01	374.26±7.21	617.83±2.63	1052.15±7.96
9	29.91±0.02	30.01±0.01	191.00±0.85	270.86±3.09	521.81±3.35
16	30.01±0.09	30.01±0.01	97.24±0.76	161.30±2.22	318.54±2.12
25	30.08±0.11	30.04±0.01	78.94±0.76	109.59±0.66	248.65±1.04
36	30.16±0.04	30.02±0.01	40.38±0.34	82.01±0.08	182.58±0.38
49	30.00±0.05	30.02±0.01	33.81±0.71	67.82±0.08	161.65±0.75
64	30.03±0.08	30.02±0.01	78.17±1.32	55.92±0.18	194.14±1.38

The average value and standard error of the timings are obtained through averaging over 8 runs on the same computing node(s). The columns corresponding to the solvers and the I/O are repeated in Table 1. For the sake of completeness we have reported here also timings for Pre-reading and Read Optics. The timings in these two columns refer to an intrinsically sequential part of the code and do not scale. They also account for a fraction of the two bottlenecks and that is why we do not have included or addressed them in the paper.

S1.2. Weak scaling tests

In this part, we show the data for the CPU-times for the weak scaling tests. For almost all simulations on BW, the average and standard deviation of the time to solution are computed over 5 runs on the same node(s). Only the simulations execute on 100 or larger computing nodes using the old code and solver have been run only once. Due to the long duration, these latter executions were very costly in terms of computing

Table S2: Strong scalability for the old reading and building routine and the KSCG solver. 16 number of threads are used per MPI rank and the data is averaged over 8 runs on the same node(s).

# MPI ranks	Pre-reading	Read optics	Reading/Building	KSCG	Total
1	25.89±0.02	25.81±0.03	336.55±6.10	5515.65±4.64	5903.90±8.59
4	29.69±0.14	29.55±0.03	374.96±9.08	1554.04±0.93	1988.24±8.75
9	29.92±0.44	30.12±0.08	413.86±3.11	830.26±0.22	1304.17±3.48
16	29.68±0.07	29.63±0.06	408.63±7.45	592.23±1.27	1060.17±7.75
25	29.75±0.09	29.59±0.06	443.46±14.78	471.94±0.31	974.74±14.74
36	29.72±0.07	30.02±0.06	491.44±12.28	427.56±0.31	978.30±12.30
49	29.66±0.05	29.84±0.01	451.09±2.46	383.55±2.708	894.15±3.53
64	29.71±0.05	29.63±0.11	450.20±2.10	359.89±0.50	869.43±2.20

time. Moreover, the variation in timings also for smaller number of computing nodes was so negligible that repeating the measurement would have brought no benefit to the statistics of the result. All executions are performed with one MPI rank and 16 ranks per computing node.

Table S3: Results of the weak scaling tests on Blue Waters for both the old and new I/O and both solvers, ChASE and KSCG. All simulations were executed with one MPI rank per node

MPI ranks	Matrix size	ChASE time (s)	STDEV (s)	KSCG time (s)	STDEV (s)	Speed up
1	38537	3188.35	10.89	5197.46	1.28	1.63
4	76887	2986.44	14.61	6701.22	2.06	2.24
9	115459	2672.35	21.04	6576.31	1.99	2.46
16	154023	4657.37	303.26	8036.14	1.37	1.73
25	192788	2443.02	17.20	8128.18	9.97	3.33
36	231011	3522.34	138.67	9072.10	1.75	2.58
49	269645	2615.52	61.03	10781.91	19.69	4.12
64	307865	3699.07	96.77	11736.11	2.99	3.17
81	346915	4771.18	97.73	12855.16	6.50	2.69
100	385183	6522.20	158.07	13755.39	-	2.11
121	423607	5408.97	111.74	15318.24	-	2.83
144	462469	4462.82	174.62	16123.97	-	3.61
169	500649	4172.64	237.95	17825.44	-	4.27

In Table S4 and S5 we report average timings and corresponding standard deviation for the procedures internal to the ChASE eigensolver over 15 repetitions on the JUWELS cluster. The labels on the columns indicates respectively:

- **Lanczos:** This a modified Lanczos algorithm to compute the approximate spectral density which is used to estimate the value of λ_1 , $\lambda_{\text{nev}+\text{nex}}$ and λ_N . This procedure is executed only once, the first time the solver is invoked.
- **Filter:** The Chebyshev filter is the computational core of the solver and the most intensive in terms of FLOPs. This is also the procedure that is most efficient since it is practically a repeated call to the **HEMM** subroutine of the BLAS library. This routines and all the remaining below are executed at each internal *while* loop of ChASE. Each repetition of the loop roughly corresponds to an iteration of the subspace projection.
- **QR:** This column corresponds to a QR decomposition of the filtered vectors outputted by the Filter. It is executed redundantly on each node.

- **RR:** The Rayleigh-Ritz step corresponds to the projection unto the subspace spanned by the filtered vectors Q outputted by the QR decomposition. It also includes the solution of the reduced eigenproblem through a standard solver from the LAPACK library and a back-transformation of the approximate eigenvectors. Both the projection and the back-transformation are executed by repeated invocation of GEMM subroutines.
- **Resid:** This label indicates the computation of the eigenpairs residual and the deflation and locking of converged vectors. Also in this case most of the computation is carried on using GEMM.

Table S4: Timings of the weak scaling tests on JUWELS for the CPU nodes. All values are averaged over 15 runs.

# MPI (p)	ChASE time (s)	Lanczos (s)	Filter (s)	QR (s)	RR (s)	Resid (s)
4	85.68 ± 1.19	18.83 ± 0.42	58.07 ± 0.99	0.90 ± 0.01	2.90 ± 0.05	2.88 ± 0.05
16	82.12 ± 1.16	19.17 ± 0.84	53.31 ± 0.75	1.80 ± 0.04	3.07 ± 0.06	3.03 ± 0.06
36	111.66 ± 0.96	19.75 ± 0.86	76.28 ± 0.79	4.37 ± 0.08	4.43 ± 0.08	4.39 ± 0.13
64	105.99 ± 1.96	21.34 ± 1.61	67.71 ± 0.64	5.79 ± 0.13	4.58 ± 0.09	4.47 ± 0.19
100	102.28 ± 3.36	23.00 ± 2.96	62.09 ± 0.35	6.40 ± 0.15	4.66 ± 0.20	4.36 ± 0.13
144	107.43 ± 2.96	24.05 ± 2.94	63.67 ± 0.67	8.10 ± 0.24	5.04 ± 0.20	4.83 ± 0.17
196	126.05 ± 4.45	28.69 ± 4.13	71.37 ± 0.43	11.91 ± 0.24	6.21 ± 0.29	5.78 ± 0.15

All the calls to the BLAS subroutines are executed on the computing node either by calls to the corresponding multi-threaded routines of the Intel MKL (Table S4) or the Nvidia CuBLAS library (Table S5). The only exception is the QR decomposition which is always executed on the CPU and not on the GPU cards. One can observe the effect of such implementation in the increasing values of the timings in the QR column as the number of computing nodes gets larger. This is a limitation of the current algorithm in the ChASE library. Future version of ChASE will feature a distributed QR decomposition and an automatic mechanism which would switch from a redundant node-level execution to a full distributed one.

Table S5: Timings of the weak scaling tests on JUWELS for the GPU nodes. All values are averaged over 15 runs.

# MPI (p)	ChASE time (s)	Lanczos (s)	Filter (s)	QR (s)	RR (s)	Resid (s)
4	33.54 ± 0.19	3.82 ± 0.04	17.37 ± 0.16	1.04 ± 0.02	0.63 ± 0.04	0.54 ± 0.01
16	31.99 ± 0.10	3.90 ± 0.07	15.87 ± 0.06	2.08 ± 0.03	0.92 ± 0.02	0.79 ± 0.01
36	49.42 ± 0.18	4.00 ± 0.05	25.05 ± 0.12	5.45 ± 0.07	1.61 ± 0.05	1.47 ± 0.05
64	45.85 ± 0.13	4.19 ± 0.04	20.88 ± 0.11	6.93 ± 0.07	2.00 ± 0.04	1.69 ± 0.04
100	44.25 ± 0.08	4.21 ± 0.05	19.48 ± 0.08	7.83 ± 0.04	2.27 ± 0.04	2.00 ± 0.09
144	48.97 ± 0.18	4.36 ± 0.07	21.18 ± 0.09	9.82 ± 0.05	2.77 ± 0.05	2.37 ± 0.05
196	59.36 ± 0.09	4.45 ± 0.07	24.26 ± 0.08	13.85 ± 0.04	3.55 ± 0.08	3.16 ± 0.11

In Table S6 we report the details of the runs of both CPU and GPU nodes of the JUWELS cluster including the number of subspace iterations and mat-vec multiplications performed. These mat-vec are a breakdown of all the single multiplications of the BSE matrix with the filtered vectors. Despite being counted as single mat-vec for the purpose of having a measure of the complexity of the execution, all the operations are carried on by multiplying the BSE matrix with a block of vectors. This strategy is at the base of the multiple invocation of the BLAS level 3 routines. The ChASE algorithm, despite being an iterative algorithm, is quite deterministic. Once a grid of computing nodes has being assigned, the solver performs the same number of iterations and mat-vec multiplications to reach convergence independently if it is executed only on CPU cores or on a hybrid combination of CPU and GPU cores. In other words the complexity of the algorithm does not change across computing platforms.

Table S6: Nodes configuration and number of iteration and mat-vec multiplications for the weak scaling tests on JUWELS for the CPU and GPU nodes.

# MPI ranks	Node level configuration				Matrix size	Number of Iterations	mat-vec multiplications
	CPU		GPU				
	# OMP	# GPU	# OMP	# GPU			
4	12	0	10	4	38537	6	8960
16	12	0	10	4	76887	5	8160
36	12	0	10	4	115459	7	11360
64	12	0	10	4	154023	6	10020
100	12	0	10	4	192788	5	9340
144	12	0	10	4	231011	5	9540
196	12	0	10	4	269645	6	10620

In Table S7 we report benchmark timings of the two MPI calls that are used within the Filter procedure using the OSU Micro-Benchmarks[S53]. Since this procedure takes a large percentage of the computing time these benchmarks give a reasonable measure of the communication overhead experienced by the ChASE library. As pointed out in Sec. 4.2, a number of factors contributes to the fluctuation of the total time to solution of the ChASE solver. It is the combination of the variation of the total number of mat-vec, subspace iterations and duration of the latency of the calls to `MPI_Allreduce` and `MPI_Ibcast` that contribute to the trend depicted in Fig. 3. For instance, the latency time for the `Ibcast` increases steadily as more MPI ranks are used, contributing positively to the total time. The same cannot be said for the latency of the `Allreduce` which benefits from a number of MPI ranks equal to a powers of two. In particular this combination of factors explains the jump in timings from 16 to 36 nodes due to all factors contributing positively, and especially the number of mat-vec performed.

Table S7: Results of the Benchmark of `MPI_Allreduce` and `MPI_Ibcast` on the JUWELS cluster obtained using the OSU Micro-Benchmarks.

#nodes	MPI Ranks	Message size	Avg. Latency (μ s)	
			<code>MPI_Allreduce</code>	<code>MPI_Ibcast</code>
1	4	16MB	12540.32	9482.64
4	16	16MB	15661.46	17102.91
9	36	16MB	21918.39	20391.34
16	64	16MB	17021.43	22392.87
25	100	16MB	23168.14	29695.72
36	144	16MB	21936.58	34585.03
49	196	16MB	23259.20	41008.10

S1.3. Dependence of the convergence rate of ChASE on `nex`

In this subsection, we illustrate the importance of choosing an `nex` value that maximizes the convergence rate of ChASE without excessively increasing the complexity of the total execution. As an illustrative example we report in Table S8 and S9 the value of some important parameters computed at the last step of the subspace iteration using both a value `nex` = 25 and `nex` = 100 for the weak scaling test on BW.

- λ_{nev} is the value of the last desired eigenvalue computed by ChASE. In both tables `nev` = 100.
- α is an estimate of $\lambda_{\text{nev}+\text{nex}}$

- β is an estimate of λ_N . This is computed by the Lanczos procedure and does not change for the remainder of the ChASE execution.
- c and e are, respectively, the center and the half-width of the interval filtered out. They are computed from the values of α and β .
- ρ_{nev} is the rate of convergence of the latest desired eigenpair. This is computed according to the following formula.

$$|\rho_{\text{nev}}| = \max_{\pm} \left\{ \left| \frac{\gamma - c}{e} \pm \sqrt{\left(\frac{\gamma - c}{e}\right)^2 - 1} \right| \right\} \quad (\text{S1})$$

Because of the design of the Chebyshev filter, such convergence rate is the worst among all sought after eigenpairs. We report the inverse of such number which represent the dampening factor: the closest to 1, the slower the eigenpair $(\lambda_{\text{nev}}, x_{\text{nev}})$ would converge to a residual below the required tolerance threshold.

We use values computed during the last iteration since they are the closest to the corresponding unknown true value of the parameter.

First, the dampening factor $\frac{1}{\rho_{\text{nev}}}$ for $\text{nex} = 100$ is in general smaller than that for $\text{nex} = 25$. This is expected and corresponds to better convergence of the iterations process as can be seen by the systematic lower number of iteration to convergence for $\text{nex} = 100$. Within the same nex , the rate of convergence shows an increasing trend as the number of computing nodes increases. Such behavior can be mainly attributed to the significant increase in β as the matrix sizes increases. Unlikely the β values, the $\alpha \approx \tilde{\lambda}_{\text{nev}+\text{nex}}$ values show fluctuations as the size of the matrix increases, the changes in both values leads to the variation in the dampening factor which, in turn, influences the time-to-solution for the ChASE solver, as already pointed out in Sec. 4.2. The observations above should be considered qualitative, as they only focus on the largest desired eigenvalue, and on the last iteration. In practice, the actual convergence of the entire subspace of eigenvectors is a bit more complicated, and it is influenced by the affective convergence rate of all the desired eigenvalues at each iteration.

Table S8: Detailed data for the convergence ratio for the largest desired eigenvalue λ_{nev} of the last step of iteration with $\text{nex} = 25$.

# nodes	λ_{nev}	α	β	c	e	$1/\rho_{\text{nev}}$	# iterations
1	3.64939	3.75894	10.08705	6.92299	3.16406	0.76921	6
4	3.64930	3.73778	13.43655	8.58716	4.84939	0.82635	5
9	3.64924	3.76372	14.38214	9.07293	5.30921	0.81278	7
16	3.64915	3.73978	16.38626	10.06302	6.32324	0.84442	7
25	3.64914	3.80541	18.13631	10.97086	7.16545	0.81183	5
36	3.64910	3.73653	19.15953	11.44803	7.71150	0.86033	6
49	3.64909	3.73887	20.79428	12.26658	8.52770	0.86504	5
64	3.64905	3.73834	21.19633	12.46734	8.72900	0.86683	6
81	3.64904	3.73833	22.62650	13.18241	9.44409	0.87162	10
100	3.64902	3.74087	22.91544	13.32816	9.58728	0.87083	10
121	3.64903	3.76850	24.78667	14.27758	10.50909	0.86016	8
144	3.64903	3.81612	26.08816	14.95214	11.13602	0.84113	7
169	3.64899	3.81917	26.75923	15.28920	11.47003	0.84194	7

S1.4. Optimization of the nex value

In this section, we describe a simple method to optimize the choice of the nex value for the sequence of eigenproblems of varying size used in the weak scaling test. First, we select a matrix at the beginning of the sequence for which the value $\text{nex} = 25$ may not be ideal. This happen to be the eigenproblem with matrix size $N = 231,011$ corresponding to an $E_{\text{cut}} = 10.54$ eV. We repeatedly solve this eigenproblem, each time

Table S9: Detailed data for the convergence ratio for the largest desired eigenvalue λ_{nev} of the last step of iteration with $\text{nex} = 100$.

# nodes	λ_{nev}	α	β	c	e	$1/\rho_{\text{nev}}$	# iterations
1	3.64939	7.17276	10.08705	8.62991	1.45715	0.14956	3
4	3.64930	7.85694	13.43655	10.64674	2.78981	0.20797	3
9	3.64924	8.61066	14.38214	11.49640	2.88574	0.19055	3
16	3.64915	3.90693	16.38626	10.14660	6.23966	0.75091	4
25	3.64914	4.33603	18.13631	11.23617	6.90014	0.64238	4
36	3.64910	4.33000	19.15953	11.74476	7.41477	0.65355	4
49	3.64909	4.32190	20.79428	12.55809	8.23619	0.66932	4
64	3.64905	3.98738	21.19633	12.59186	8.60448	0.75615	4
81	3.64904	3.91196	22.62650	13.26923	9.35727	0.78938	4
100	3.64902	3.97604	22.91544	13.44574	9.46970	0.76947	8

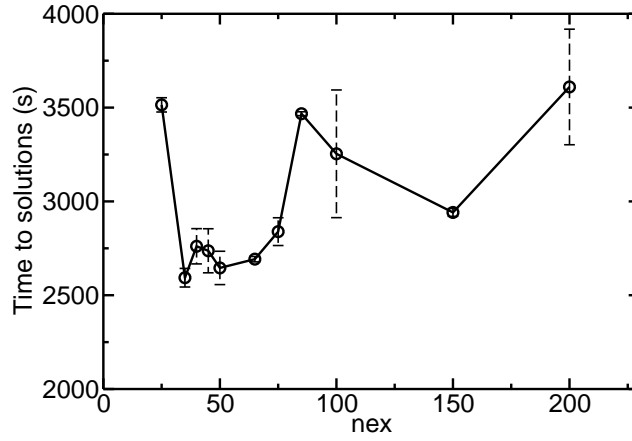


Figure S1: Optimization of the nex value for the 36 nodes matrix in the weak scaling test. All data points are averaged over three runs, with the standard deviation plotted in dashed lines. The computational walltime first drops due to better convergence, then increases due to large size of the eigenvectors.

slightly increasing the nex value. We expect to find a value of nex for which the computing time of ChASE is minimized. Result of such a test are shown in Fig.S1. Inspecting the plot, the interval $\text{nex} = 35 - 50$ seems to be the one within which the time-to-solution is likely to be minimal. We artificially set such a minimal value to be 40. We define such a value to be the lower end of a linear regression of nex and label it as nex_{low} . Correspondingly we label $E_{\text{cut}} = 10.54$ as $E_{\text{cut-low}}$. In order to avoid consuming too much computational time, we limit our regression to $E_{\text{cut}} = 12.82$, which we label as $E_{\text{cut-high}}$, and calculate the corresponding values of nex for intermediate E_{cut} values using the following formula

$$\text{nex} = \text{nex}_{\text{low}} + \frac{\text{nex}_{\text{high}} - \text{nex}_{\text{low}}}{E_{\text{cut-high}} - E_{\text{cut-low}}} \times (E_{\text{cut}} - E_{\text{cut-low}}). \quad (\text{S2})$$

Not knowing a priori the value of nex_{high} , we choose two arbitrary values for $\text{nex}_{\text{high}} = 100, 150$, and report the regressed value of nex for intermediate values of E_{cut} in Tab.S10. We then tested these values by solving the corresponding eigenvalue problems with them and comparing the time-to-solution to the one measured for $\text{nex} = 25, 100$ across all problems. The results are plotted in Fig.S2. We observe that the nex values calculated by regressions present an overall improvement with respect to the computing time when $\text{nex} = 25$ is used. However, the same cannot be said when $\text{nex} = 100$ is used across the board.

Table S10: nex values computed via linear interpolation between $\text{nex}_{\text{low}} = 40$ and $\text{nex}_{\text{high}} = 100, 150$, respectively.

# nodes (processors)	E_{cut} (eV)	$\text{nex}_{\text{high}} = 100$	$\text{nex}_{\text{high}} = 150$
36	10.54	40	40
49	11.15	50	58
64	11.73	59	75
81	12.30	68	91
100	12.82	76	106

While this experiment shows the potential to estimate the correct value of nex for increasing sizes of BSE Hamiltonians, it also illustrates the non-linear behavior of the solver as the matrix becomes larger. In general, it is advisable to increase the nex value as the matrix size increases, due to the fact that the largest eigenvalue λ_N tends to increase, leading to the worsening of the convergence rate. However, linear scaling of the nex value is probably not ideal. The effectiveness of nex is mostly influenced by the distribution of gaps in the spectrum of the eigenproblem, which is by no means a linear function. Nonetheless, maintaining the same value of nex across the board is definitely not advisable and a rule of thumb based on some sort of simple regression model can save computing time for the user of ChASE.

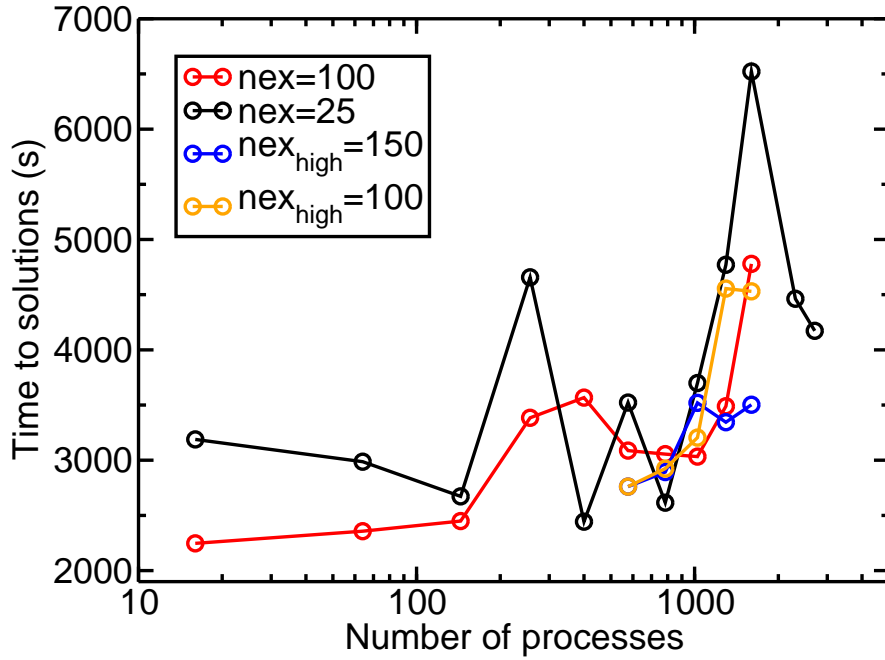


Figure S2: The effect of varying nex value across different matrix sizes with linear interpolation (orange and blue) and the comparison with the weak scaling test with fixed nex (black and red). For both orange and blue curves, $\text{nex}_{\text{low}} = 40$, obtained through the test in Fig.S1.